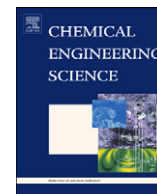




ELSEVIER

Contents lists available at ScienceDirect

## Chemical Engineering Science

journal homepage: [www.elsevier.com/locate/ces](http://www.elsevier.com/locate/ces)

## Porometry, porosimetry, image analysis and void network modelling in the study of the pore-level properties of filters

Christopher M. Gribble<sup>a</sup>, Graham Peter Matthews<sup>a,\*</sup>, Giuliano M. Laudone<sup>a</sup>, Andrew Turner<sup>a</sup>,  
Cathy J. Ridgway<sup>b</sup>, Joachim Schoelkopf<sup>b</sup>, Patrick A.C. Gane<sup>b,c</sup>

<sup>a</sup> School of Geography, Earth and Environmental Sciences, University of Plymouth, Drake Circus, Plymouth PL4 8AA, UK

<sup>b</sup> Omya Development AG, CH-4665 Oftringen, Switzerland

<sup>c</sup> Aalto University, School of Chemical Technology, Department of Forest Products Technology, P.O. Box 16300, 00076 Aalto, Finland

## ARTICLE INFO

## Article history:

Received 28 February 2011

Received in revised form

4 May 2011

Accepted 9 May 2011

## Keywords:

Filtration

Porous media

Mercury porosimetry

Mathematical modelling

Membranes

Porometry

## ABSTRACT

We present fundamental and quantitative comparisons between the techniques of porometry (or flow permporometry), porosimetry, image analysis and void network modelling for seven types of filter, chosen to encompass the range of simple to complex void structure. They were metal, cellulose and glass fibre macro- and meso-porous filters of various types. The comparisons allow a general re-appraisal of the limitations of each technique for measuring void structures. Porometry is shown to give unrealistically narrow void size distributions, but the correct filtration characteristic when calibrated. Shielded mercury porosimetry can give the quaternary (sample-level anisotropic) characteristics of the void structure. The first derivative of a mercury porosimetry intrusion curve is shown to underestimate the large number of voids, but this error can be largely corrected by the use of a void network model. The model was also used to simulate the full filtration characteristic of each sample, which agreed with the manufacturer's filtration ratings. The model was validated through its correct *a priori* simulation of absolute gas permeabilities for track etch, cellulose nitrate and sintered powder filters.

© 2011 Published by Elsevier Ltd.

### 1. Introduction

We present a critique of the limitations of single-technique characterisations of the void space of porous media, and a quantitative investigation of the additional information, which can be gained from a Cartesian void network model. The experimental samples are metal, cellulose and glass-fibre macro- and meso-porous filters of various types.

For purposes of discussion, it is convenient to categorise void space architecture into four levels. The primary structure of a porous material is taken to be the distribution of void sizes, the secondary structure the connectivity of these voids, the tertiary structure the relationship between the sizes of voids and the sizes of their immediate connecting neighbours, and the quaternary structure the size auto-correlations and gradations over the sample as a whole. These different levels of structure contribute to important properties of the sample, such as its filtration efficiency and capacity (Price et al., 2009), absorption and wetting characteristics (Ridgway et al., 2001; Wallqvist et al., 2009), and the adsorption and diffusion of pore fluids (Laudone et al., 2008;

Meyers et al., 2001). The quaternary structure determines the anisotropy of these characteristics relative to the direction of application or flow of fluids.

In this work, we use mercury porosimetry (Calvo et al., 1995), porometry (Calvo et al., 1995; Li et al., 2006; MiettonPeuchot et al., 1997) and scanning electron microscopy (SEM) with image analysis (Ziel et al., 2008). In mercury porosimetry the volume of mercury intruded into a porous sample is measured at increasing applied pressures, allowing time for equilibrium to be established at each pressure. It is a popular method for the characterisation of mesoporous and macroporous structures (Lowell et al., 2004; Thommes et al., 2008), and inferences about the surface texture of the macropores can be made from measuring the extrusion of mercury as the applied pressure is released (Rigby and Chigada, 2010).

Porometry, also referred to as flow permporometry, is a non-destructive technique used for quality control purposes in the filtration industry (MiettonPeuchot et al., 1997). It involves the expulsion of a fully wetting fluid from a saturated porous medium by increasing the gas pressure, with higher gas pressures relating to smaller pore diameters. The flow rates at particular pressures are compared to flow rates at corresponding pressures in a 'dry' run, carried out after all the wetting fluid has been expelled in the initial run. Additional information may be obtained by adding

\* Corresponding author. Tel.: +44 1752 584798; fax: +44 1752 584790.

E-mail address: [pmatthews@plymouth.ac.uk](mailto:pmatthews@plymouth.ac.uk) (G.P. Matthews).

liquid while the run is proceeding (Kumar and Chakarvarti, 2008). A recent work by Mourhatch et al. (2011) uses porometry to determine the pore size distribution of silicon carbides. They use as a starting point the bundle of capillary tubes approximation, described in more detail below. They show that by invoking a 3D invasion percolation model, a good fit to experimental porometry results can be obtained. However, the results are not cross-checked against other experimental methods, as in the present case.

SEM can be used to image the surfaces of porous materials, with its limited depth of field providing some information in the third dimension. Two-dimensional image analysis of the micrographs allows a quantitative assessment of microstructure, as well as other characteristics such as defects in construction (Rasband, 2008).

Additional experimental techniques are available but not used in this work, including nuclear magnetic resonance (NMR) (Gane et al., 2004; Matthews et al., 2006; Rigby et al., 2002), micro-focus X-ray (MFX) imaging (Rigby et al., 2002) and gas adsorption, which is more appropriate for nanoporous materials (Lowell et al., 2004; Ravikovitch and Neimark, 2002).

The network model, 'Pore-Cor', has been described in previous publications (Price et al., 2009). In this work, we apply it for the first time to porometry, which necessitates an extrapolation of the experimental data from the instrument. Pore-Cor has been previously used to model a range of materials such as soil (Peat et al., 2000), sandstone (Matthews et al., 2006), catalysts and paper coatings (Laudone et al., 2005; Ridgway and Gane, 2002). The network model has also been used as a predictive tool for the study of absorption, diffusion and filtration (Laudone et al., 2008; Price et al., 2009; Ridgway and Gane, 2002). A comparison between image-analysed micrographs and simulated microtoming showed that the traditional interpretation of mercury porosimetry grossly underestimated the void sizes of a range of sandstones, but that this could be compensated by modelling (Matthews et al., 2006).

There have been many previous multi-technique investigations of pore structure and pore architecture. A previous comparison of porosimetry and porometry showed that the latter is skewed towards smaller pores (Calvo et al., 1995; Li et al., 2006), as confirmed below, and Rigby and Daut (2002) and Rigby et al. (2002) have also carried out comparisons. However, multiple techniques are usually combined to give structures over a wider range of void sizes, rather than being critically compared. For example, mercury porosimetry and nitrogen sorption have been used to measure macroscopic ( $> 10 \mu\text{m}$ ) and microscopic ( $< 10 \mu\text{m}$ ) voids separately (Rigby, 2000), and SEM and nitrogen adsorption have been used in the study of  $\text{SiO}_2$  thin films (Sel et al., 2007). Rocks (Tsakiroglou et al., 2009) and soils have also been similarly studied, with the structure expressed as primary pores and throats, and a secondary fractal pore system.

## 2. Theoretical considerations regarding porosimetry and porometry

Using the Laplace equation it is possible to calculate the size of a cylindrical pore-throat ('throat') intruded by a non-wetting liquid applied at a pressure  $P$  relative to the evacuated void space within a sample:

$$d = -\frac{4\gamma \cos \theta}{P} \quad (1)$$

Mercury intrusion measures the volume  $V$  of mercury intruded at a pressure  $P$ , corresponding to a throat diameter  $d$ . Mercury typically has a mercury/solid/vacuum contact angle  $\theta$  of between

$130^\circ$  and  $140^\circ$  and interfacial tension  $\gamma$  of  $0.485 \text{ Nm}^{-1}$  (van Brakel et al., 1981).

A frequent, usually implicit, approximation is to assume that the void space comprises a bundle of aligned capillary tubes. Suppose for purposes of illustration that there are  $n_1$  such tubes of diameter  $d_1$  and length  $l_1$ ,  $n_2$  of diameter  $d_2$  and length  $l_2$  and  $n_3$  of diameter  $d_3$  and length  $l_3$ , where  $d_1 > d_2 > d_3$ . We assume that  $d_1$ ,  $d_2$  and  $d_3$  are logarithmically distributed, i.e. that  $d_1/d_2 = d_2/d_3$ , as typically found for natural samples. Suppose that there is a constant relationship between the diameters  $d$  of each feature and their lengths  $l$ , such that  $l = sd^m$ , where  $s$  and  $m$  are assumed constant for all features. Suppose mercury at a pressure  $P_2$  is applied, where  $-((4\gamma \cos \theta)/d_3) > P_2 > -((4\gamma \cos \theta)/d_2)$ . Then a volume  $V_{P_2}$  of mercury will intrude all the tubes of diameter  $d_1$  and  $d_2$ , where by simple geometry:

$$V_{P_2} = \frac{n_1 \pi d_1^2 l_1}{4} + \frac{n_2 \pi d_2^2 l_2}{4} = \frac{s\pi}{4} (n_1 d_1^{2+m} + n_2 d_2^{2+m}) \quad (2)$$

Analogously, if there is an increase to a pressure  $P_3 > -((4\gamma \cos \theta)/d_3)$ , such that features of size  $d_3$  are intruded, then

$$V_{P_3} = \frac{s\pi}{4} (n_1 d_1^{2+m} + n_2 d_2^{2+m} + n_3 d_3^{2+m}) \quad (3)$$

For any applied pressure,  $P_N$ , noting that the distribution of the  $N$  sizes is discrete rather than continuous

$$V_{P_N} = \frac{s\pi}{4} \sum_{i=1}^N n_i d_i^{2+m} \quad (4)$$

Almost universally in the literature, the first derivative of the porosimetry intrusion curve  $dV/d(\log_{10} d)$  is calculated, as shown schematically in Fig. 1, which we will refer to simply as the gradient. However, remembering that  $d_i$  is logarithmically distributed, from Eq. (3):

$$\frac{dV_{P_N}}{d(\log_{10} d)} \simeq \frac{(2+m)s\pi}{4} \sum_{i=1}^N n_i d_i^{1+m} \propto nd^{1+m} \quad \text{for } s, m \text{ const} \quad (5)$$

i.e. not that  $dV_{P_N}/d(\log_{10} d) \propto n$  only, as is almost universally assumed in the literature. The persistence of the wrong assumption is based on the partial, but unquantified, cancellation of two implicit approximations, namely, this assumption of number rather than volume, which over-estimates the numbers of voids of larger sizes, and the ignoring of shielded pore space, which underestimates voids of larger sizes. Shielded pore space is that for which the only access is via a throat of smaller diameter (Fig. 2(a) and (b)).

When carrying out mercury porosimetry, the breakthrough of mercury from one side of the sample to the other occurs close to the point of inflection of the mercury intrusion curve at a breakthrough pressure  $P_{bk}$ , equivalent to a breakthrough diameter  $d_{bk}$  via Eq. (1). As illustrated in Fig. 1, the volume intruded at  $P_{bk}$  (diameter  $d_{bk}$ ) is generally around 50% of the total intrusion volume.

Porometry also uses Eq. (1), with an assumed contact angle of  $180^\circ$  for air against a wetting liquid, and the assumption that the gradient, as defined above, gives the relative number of features of a certain size  $d$ . However, in the case of porometry, measurement does not start until the bubble point pressure, corresponding to a size  $d_{bp}$  via Eq. (1), at which gas first breaks through the sample. At this point, gas has already displaced fluid from all features larger and upstream of those controlling the breakthrough flow path through the sample. The porometry bubble point ( $P_{bp}$ ,  $d_{bp}$ ) therefore corresponds to the breakthrough point ( $P_{bk}$ ,  $d_{bk}$ ) in mercury intrusion. Consequently, the characteristic porometry curve covers only void sizes smaller than  $d_{bp}$ , and its traditional interpretation exaggerates the number of smaller void

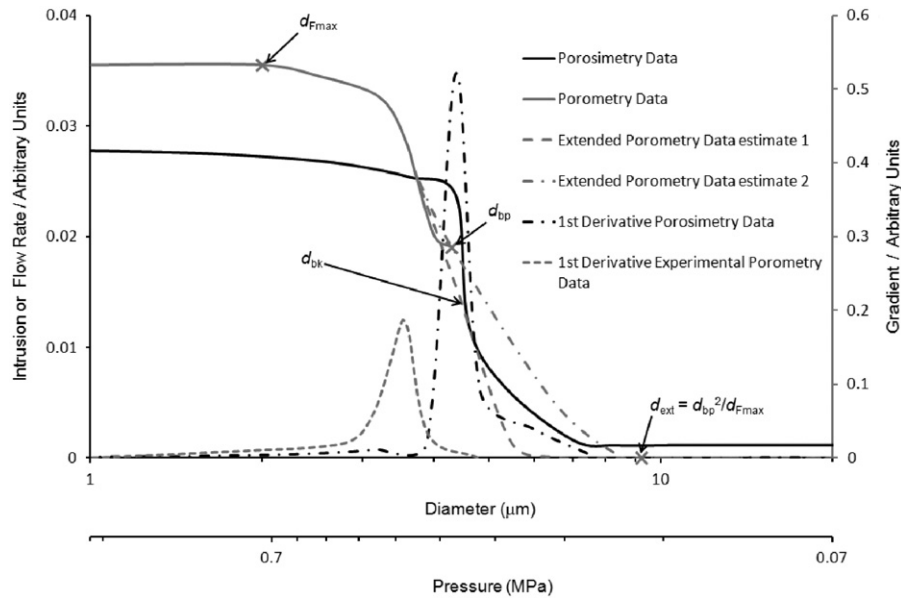


**Fig. 1.** Schematic graph showing how extrapolated porometry data should compare with mercury intrusion data, and how mercury porosimetry and porometry data are interpreted using the capillary bundle model.

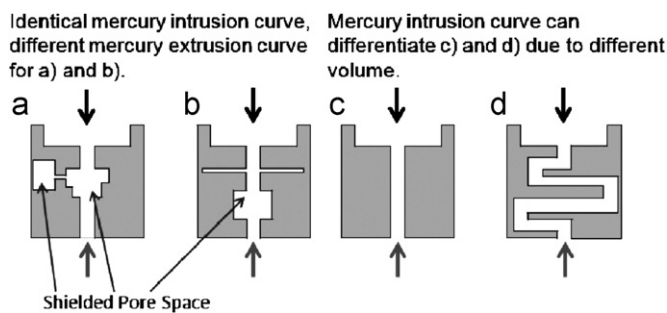


**Fig. 2.** Comparison of how mercury porosimetry and porometry probe the pore architecture of schematic structures with simple quaternary level pore architecture. Mercury for standard porosimetry is applied in the direction of the black and grey arrows, and for shielded mercury porosimetry in the direction of the grey arrows only. Air, for porometry, is applied in the direction of the black arrows. Porometry would not be able to differentiate between the four different structures.

sizes relative to porosimetry. Once the bubble point has been reached, air flows through the sample in a totally different way from mercury. Assuming that the flow is laminar, it will obey Poiseuille's equation, such that the volumetric flow rate  $Q$  of the gas is

$$Q = \frac{\Delta P \pi d^4}{128 \eta l} \quad (6)$$

where  $\Delta P$  is the pressure differential across the sample, equated to  $P$  in Eq. (1), and  $\eta$  is the kinetic viscosity of the gas. Roughness will affect the validity of Poiseuille's relationship in Eq. (6), as will constrictions and other deviations from a cylindrical geometry. By analogy with Eq. (2) and assuming aligned capillary tubes

$$Q_{APN} = \frac{\Delta P_N \pi}{128 \eta} \sum_{i=1}^N \frac{n_i d_i^4}{l_i} = \frac{\Delta P_N \pi}{128 \eta S} \sum_{i=1}^N n_i d_i^{4-m} \propto n d^{4-m} \quad (7)$$

In porometry, the absolute flow  $Q$  at a particular differential pressure, rather than the gradient differential of the intrusion curve as in porosimetry, is used to find the void size distribution, and almost universally it is assumed that  $m=2$  in Eq. (7).

However, equating the proportionalities in Eqs. (5) and (7),  $m=3/2$  is the one condition whereby porosimetry and porometry deliver the same proportional distribution.

Shielded pore space is largely ignored by porometry (Fig. 2). For filtration purposes, this shielded pore space will add to the holding capacity but not greatly affect the filtration size characteristics. So, porometry is valid for the measurement of filtration characteristics.

Fig. 2(a) and (b) show cross-sections of structures with different pore geometries, but with the same initial mercury intrusion (percolation or drainage) characteristics because there is initially an identical size/volume progression from large to smaller void features within the void network. However, mercury extrusion (imbibition) would detect the difference between the networks if the single entry ('ink bottle') pore to the left in Fig. 2(a) is much larger (typically more than five times larger) than its entry throat so that snap-off occurs (Dawe and Egbogah, 1978). Structures (c) and (d) have the same diameter throat with different volumes and tortuosities. In theory, mercury porosimetry should be able to detect the difference between these structures, because for structure (d) there would be greater volume of piston flow down the throat once the required pressure was reached according to Eq. (1). In real samples, however, differences of this type are more subtle and difficult to detect.

The application of porometry to the samples in Fig. 2 would involve initial application of a proprietary wetting fluid in the direction of either the black or grey arrows, which is then held in the structures by capillarity. Air, subsequently applied in the direction of either the black or grey arrows, would break through all the structures at the same pressure, so would be unable to differentiate between them. The flow rates through the dry structures, largely controlled by the smallest throats within critical flow pathways, would also be identical. So, porometry would suggest a distribution of smaller voids than porosimetry, as found for real samples (Calvo et al., 1995; Li et al., 2006).

If in shielded porosimetry the tops of the schematic samples are resin embedded, mercury will intrude in the direction of the grey arrows only (Fig. 2). So, it would mimic porometry and be unable to differentiate between the four structures. However, the fact that the results of standard porosimetry, and those of porometry or shielded porosimetry, were different, would identify that the structures had a

quaternary level of pore architecture—in this case that they had one face with large pores, and one with small.

A quantitative comparison between porometry and porosimetry can be made using the void network model. In order to derive directly comparable void structures from the two techniques, we assume that the porometry curve commences at 50% of the intruded volume by analogy with the mercury porosimetry curve, as shown in Fig. 1. We also specify one point  $d_{\text{ext}}$  on the extended porometry asymptote at low pressure/large size, the same distance above the bubble point  $d_{\text{bp}}$  on the logarithmic axis as the high pressure/small size asymptote  $d_{\text{Fmax}}$  is below it, as shown in Fig. 1, so that:

$$d_{\text{ext}} = d_{\text{bp}}^2 / d_{\text{Fmax}} \quad (8)$$

The result is that we have extended the porometry curve so that it is equivalent to a porosimetry curve. However, there are no experimental points between  $d_{\text{bp}}$  and  $d_{\text{ext}}$  for the model to fit. Therefore, the model is free to simulate any mercury intrusion characteristic between those two points, and so there can be wide variations between different stochastic realisations of the model, illustrated as estimates 1 and 2 in the figure (and later in Fig. 12). This is a direct consequence of porometry omitting much of the larger detail of the pore structure. The stochastic variation could be reduced by comparing the simulated permeability of different stochastic realisations with the permeability measured by the porometer during its dry runs.

### 2.1. Network model

The simulated void network structure within the Pore-Cor network model comprises cubic unit cells connected infinitely in each Cartesian direction. Each unit cell itself comprises a  $10 \times 10 \times 10$  array of pores, with up to 3000 interconnecting throats, arranged in a regular Cartesian array with periodic boundary conditions, such that fluid exiting one face of a unit cell enters the opposite face of the adjoining replicate unit cell (Fig. S5). An annealed amoeboid simplex is used to find a structure that closely matches the porosimetry or porometry characteristics of an experimental structure by varying various fitting parameters controlling the geometry of the network. The model takes an implicitly Bayesian approach, by initially assuming typical relationships between the sizes of pores and their adjoining throats. The fitting parameters are termed connectivity, pore skew, throat skew, throat spread and correlation level. Connectivity is the average number of throats per pore. Pore skew bulks up pores relative to the sizes of adjoining throats. The correlation level varies from zero (completely random) to 1. The value 1 represents a chosen ordered structure such as a vertically layered structure (as in the present work), a horizontally layered structure, or a structure with spherical zones of small or large voids. The type of ordered structure is chosen by the user, in the knowledge that an unsuitable structure type will not allow a fit to the experimental data. Throat spread widens the spread of the logarithmically distributed throat size distribution of throat sizes, described by an Euler beta function. It also determines whether the distribution is unimodal or bimodal. Throat skew controls the skew of the Euler beta distribution. A full mathematical description of these parameters has been published recently (Matthews et al., 2010).

Application of the Pore-Cor model to porometry has the advantage of estimating all the void space of a porous sample, and hence its holding capacity. Absolute numbers of features per unit volume of sample may be calculated or absolute volumes of features at each size. A direct simulation of the filtration capacity of the modelled structure can be calculated, which describes the gradual increase of differential pressure, decrease in holding capacity and increase in filtration capability as the filter captures increasing numbers of particles (Price et al., 2009).

Validation of the model was made by comparing the absolute gas permeabilities of the modelled structures, calculated using an incompressible fluid trickle-flow approximation (Matthews et al., 1995), with experimental measurements from the porometer, as described below.

## 3. Experimental

### 3.1. Materials

Three filters from Whatman were investigated: a Nucleopore track etch membrane, with a filtration rating of  $1.0 \mu\text{m}$  (lot number 5102005), a grade 1 filter paper with a filtration rating of  $11 \mu\text{m}$  (catalogue number 1001 042), and a cellulose nitrate filter with a filtration rating of  $0.45 \mu\text{m}$  (reference number 7184-004 lot number FN0056-1).

Two filters prepared by the Porvair Filtration Group were studied. One was a stainless steel mesh filter '3AL3' that had a filtration rating of  $3 \mu\text{m}$ . The second was a specially constructed compound filter comprising two different stainless steel sinters. One was coarse with pore features greater than  $20 \mu\text{m}$ , and the other had a pore size distribution of approximately  $0.5\text{--}1.5 \mu\text{m}$ . A stainless steel sinter with a pore size of  $2\text{--}5 \mu\text{m}$  from Aegis Advanced Materials Ltd., U.K, was also characterised. The seventh sample was a Fisherbrand GF300 Glass Fibre Filter with a filtration rating of  $0.7 \mu\text{m}$ .

Different samples of each filter type were used for each experiment, because the experiments required irreversible treatment of the samples, such as gold coating or intrusion of mercury. It was assumed that all the different instances of each sample type were identical. This assumption was validated by running all porometry measurements in triplicate, which showed negligible difference between the replicates.

### 3.2. Mercury porosimetry

Mercury porosimetry was performed on a Micromeritics AutoPore III 9420 or Autopore IV 9520 mercury porosimeter (Micromeritics Corporation, USA) with a pressure table from 0.01 to 400 MPa, following ISO 9001:2008 protocols. The equilibrium time for each pressure point was 30 s. The pressure values were converted into pore diameters using the Laplace equation, Eq. (1). The pore diameter was subsequently plotted against the gradient of the intrusion curve (as defined previously) to give a volumetric distribution of pore size.

### 3.3. Porometry

Porometry was performed on a Porvair Porometer 4 (Porvair Filtration Group, UK), with control software written by Laudone to control the instrument and carry out the extrapolation described earlier. The sample chamber had a diameter of 25 mm. The samples were first wetted by soaking in the proprietary wetting fluid, Porofil, supplied by Beckman Coulter. Porofil has a low vapour pressure  $0.4 \text{ kPa}$ , a low reactivity and a low interfacial tension of  $0.016 \text{ Nm}^{-1}$ , and it is assumed the samples are fully wetted, i.e.  $\theta=0$ , Eq. (1) (Calvo et al., 1995; Li et al., 2006; MiettonPeuchot et al., 1997; Solcova et al., 2006). The samples were placed in the sample chamber, additional Porofil was added to ensure the samples were saturated, and then the sample chamber was sealed. A wide range of applied pressure was chosen initially, and then refined to that appropriate for the particular sample. The subsequent dry run, against which the wet run was compared, gave the flow rates of gas through the dry sample at applied pressure within the chosen range, and hence a direct

measure of absolute gas permeability, which was used to validate the model. Subtraction of the wet flow run from the dry flow run gave the net hold-ups of flow at each pressure, which were converted to pore diameters via Eq. (1).

### 3.4. Scanning electron microscopy and image analysis

Scanning electron microscopy was performed on a Jeol JSM-5600 LV or Jeol JSM-6100 SEM (Jeol Ltd, Japan) under high vacuum conditions in secondary electron mode. The non-conductive samples were coated with gold before imaging. The SEM images were analysed using ImageJ (Rasband, 2008) to obtain the feret diameter of the porous features, where the feret diameter is the longest direct distance between any two points on the boundary of the void feature. Size calibration was based on the SEM image scale-bars. The images were thresholded using ImageJ to distinguish between void space and material. The thresholding also removed imperfections such as scratches on the surface. Feret diameters were converted to histograms to combine the size distributions obtained from a minimum of eight images from each sample.

## 4. Modelling

The mercury porosimetry samples were corrected for the blank chamber run, mercury compression and compressibility of the sample using Pore-Comp (Gane et al., 1996). No allowance was made for any distortion of the sample by the intruding mercury, which would be likely in the case of the glass fibre and paper filters. Compression and distortion of the samples under the maximum pressure applied during porometry (600 kPa) was assumed to be insignificant.

Porosimetry and porometry sample data were modelled with Pore-Cor Research Suite v6.31 to generate a stochastic series of five void structures, all of which closely matched the experimental data. The most representative stochastic realisation of the five (i.e. with all the parameters closest to the mean of the set of five) was chosen for comparison with the experimental pore size distribution and filtration results (Tables S1–S7 in the Supplementary Information). Filtration was simulated by a succession of single particles, randomly chosen from an arbitrary distribution of sizes close to the quoted filtration rating (Price et al., 2009). Each particle followed a stochastic path through the medium, with the highest probability of it being in the path of maximum flux (Fig. S5). Any particle encountering a feature smaller than its own diameter was trapped (strained), and blocked the feature, whereupon the flow paths and pressure differential across the sample were recalculated prior to entry of the next particle.

The model was validated by comparing the permeability of the modelled structure, calculated with an incompressible fluid approximation, with that of the experimental sample measured directly using the porometer. For permeability all five stochastic realisations were used, and the mean and standard deviation of the five permeabilities, expressed on a logarithmic scale, was used for comparison with experiment.

## 5. Results and comparisons

### 5.1. Characterisations

All samples were characterised by appropriate combinations of porometry, porosimetry, scanning electron microscopy and image analysis. The results are reported below and in the appendices. However, they do not include measurements of  $s$  and  $m$  (Section 2).

Those would require a porosimeter that was so sensitive that the intrusion of individual features could be detected, and we are not aware that measurements from any such device have been reported in the literature.

### 5.2. Network model

All the experimental porosimetry and porometry results were fitted using the Boltzmann-annealed amoeboid simplex of Pore-Cor Research Suite version 6.31, with stochastic generations handled as described above (Tables S1–S7).

### 5.3. Comparisons

The simplest void structure was that of the Whatman track etch membrane, an SEM of which is shown in Fig. 3. Image analysis gave a porosity of 26.8%, a modal feature size of  $0.8\ \mu\text{m}$  with a distribution of  $0.5\text{--}2.5\ \mu\text{m}$  (Fig. 4). The void sizes obtained directly from porosimetry cover a narrow size range around  $0.7\ \mu\text{m}$ . The range for porometry is even smaller at around  $1.1\ \mu\text{m}$ , very close to the manufacturer's filtration rating of  $1\ \mu\text{m}$ . It can be seen that modelling spreads the distributions, in

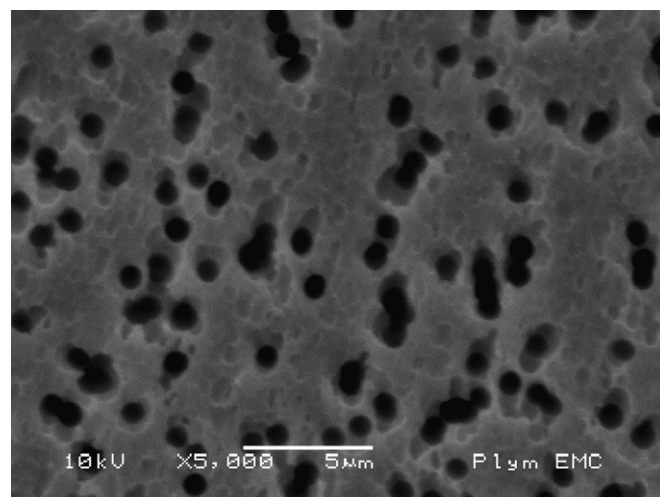


Fig. 3. SEM image of  $1\ \mu\text{m}$ -rated track etch membrane, with  $5\ \mu\text{m}$  scale bar.

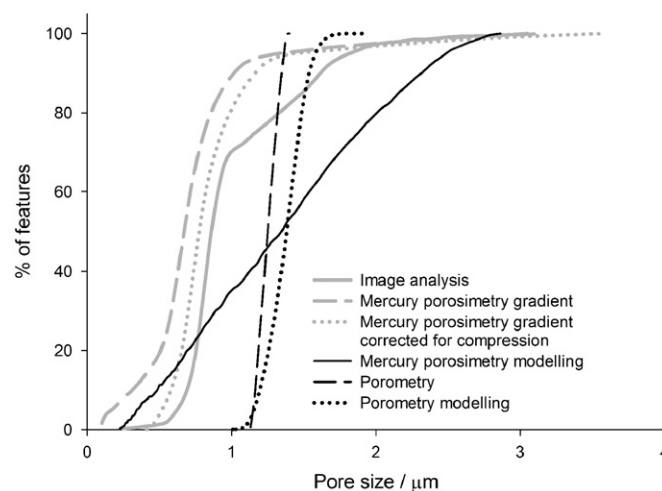


Fig. 4. Pore size distribution for a Whatman track etch membrane determined using image analysis, mercury porosimetry and porometry with a pore size distribution calculated by the Pore-Cor model for porometry and mercury porosimetry.

the case of mercury porosimetry nearly to 3  $\mu\text{m}$ . Fig. 3 shows that these larger sizes arise from overlapping pore tracks. Individual overlaps may not extend through the entire thickness of the sample, so do not alter the filtration characteristic. This is confirmed using the model to simulate filtration (Price et al., 2009; Fig. 5). The relative pressure drop axis shows the pressure build up, and the vertical axis the accompanying increase in filter efficiency, as an increasing number of particles in the range 0.5–0.8  $\mu\text{m}$  are filtered out. Even though the modelled voids extend to 3  $\mu\text{m}$ , it can be seen that all particles above 0.8  $\mu\text{m}$  experience 100% capture efficiency, in accord with the manufacturer's 1  $\mu\text{m}$  filtration rating. The filtration characteristic surface in Fig. 5 is less monotonic than for other filtration simulations, shown in the Supplementary information.

The next most complicated sample was the Aegis stainless steel powder sinter. Image analysis of the SEM (Fig. S1) gave a unimodal distribution of pore sizes over the range 0.5–20.0  $\mu\text{m}$  with a mode near 2.5  $\mu\text{m}$  (Fig. 6). Whereas the gradient of the mercury intrusion measurements gave a distribution which is too sharp, the modelled curve is closer to the image analysis result. Image analysis also shows, as large features > 8  $\mu\text{m}$ , the surface

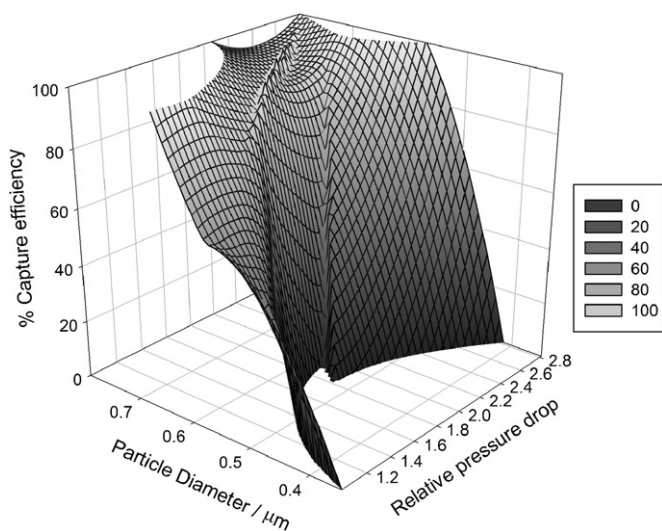


Fig. 5. Filtration simulation for track etch membrane, filtration rating 1  $\mu\text{m}$ .

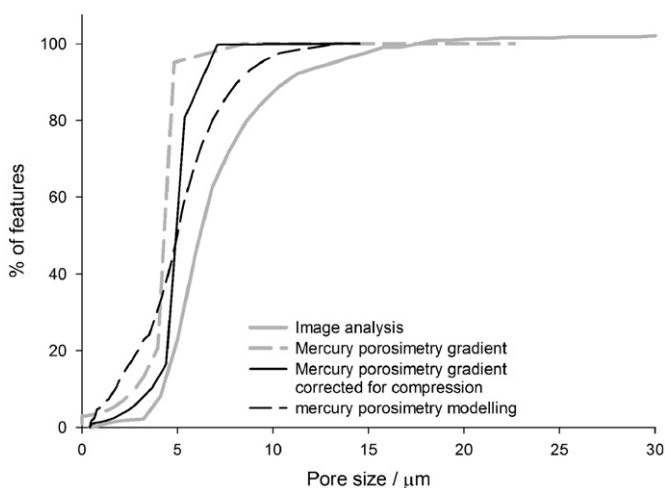


Fig. 6. Pore size distribution of Aegis stainless steel sinter determined using mercury porosimetry, image analysis and a pore size distribution calculated using Pore-Cor.

striations (Fig. S1). These striations are undetected by mercury porosimetry because they fill with mercury on contact.

Fig. 7 shows the extent to which these methods can correctly measure the void structure of a compound sinter comprising two entirely different individual sinters. The image analysis of the images of each different side of the compound sinter (Figs. S2 and S3) gave the two entirely different ranges shown in Fig. 7. Porometry was impossible, because the sinter was smaller than the sample chamber, so was simulated by resin embedding the larger-pore side of the sinter and then carrying out mercury porosimetry. As expected, this, and its modelling, agrees with the image analysis of the finer surface (Fig. 7). The mercury porosimetry of the whole sample straddles both size distributions. Modelling of the porosimetry gives a more realistic distribution at the larger scale, relative to image analysis, than porosimetry alone.

For the other, more complicated filters, image analysis of two-dimensional electron micrographs could not yield useful information about 3D structure. The comparisons for these filters (Figs. 8–11 and S4, S7, S9, S11 and S12) all show the same relationships: a narrow size range deriving from porometry, and hence narrow range for modelled porometry, a wider range derived from the gradient of the mercury intrusion curve, and an even wider range from modelled porosimetry. Although there are no image analysis results against which to check the accuracy of these estimates, all the modelled structures gave realistic filtration characteristics relative to the manufacturers' filtration ratings (Figs. S6, S8, S10 and S13).

#### 5.4. Model validation

The validity of the model was tested by comparing the absolute gas permeabilities measured with the porometer with those derived from an *a priori* simulation using the model's incompressible trickle-flow approximation (Matthews et al., 1995). The estimated uncertainty of the experimental measurement was around 2%, which is negligible on the logarithmic permeability axis used in Fig. 12. The track etch membrane comprised an array of single cylindrical capillaries in what we refer to as the *z*, or effective *z* direction. However, the model is isotropic, and therefore simulated the track edge membrane with additional features in the *x* and *y* directions, which did not exist in the sample. The porosity of the simulated structure was therefore increased by 3.2% absolute so that the volumes of the modelled features in the *z* direction were identical to those in the sample.

Fig. 12 shows that there is good agreement between the experimental and modelled permeabilities of the track etch membrane (TEM), and agreement to within 2 standard deviations for the skeletal clathrate structure of the Whatman cellulose nitrate filter (WCN). There is also agreement to within one and three standard deviations for the fibrous Whatman filter paper (WFP). However, for the glass fibre filter (GFF) and the stainless steel mesh filter (3AL3), there is no agreement because the model is unable to reproduce the complexities of the geometry of the fibrous networks, and of the gas flow through them.

## 6. Discussion and conclusion

Fig. 4 showed very close agreement between the porometer void size distribution, centred on 1.1  $\mu\text{m}$ , and the manufacturer's filtration rating of 1.0  $\mu\text{m}$ . However, this agreement is artificial. Porometry typically uses a proprietary fluid, in this case 'Porofil'. Although the characteristics of the fluid are quoted in terms of interfacial tension and contact angle as above, Eq. (1), these properties derive from a prior calibration against a track etch membrane rather than a measure of the properties of the fluid.

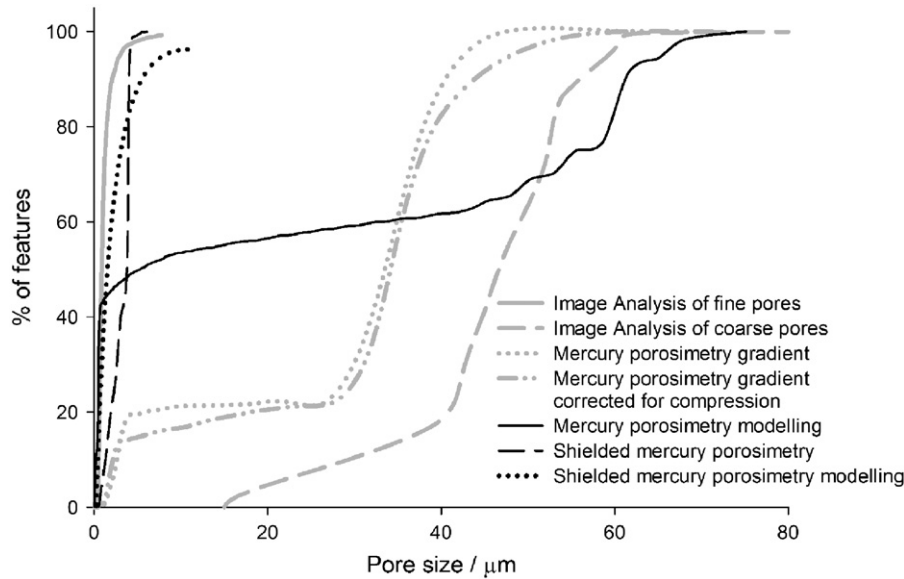


Fig. 7. Pore size distributions of a 3  $\mu\text{m}$  rated Porvair stainless steel sinter using mercury porosimetry, shielded mercury porosimetry and SEM and image analysis.

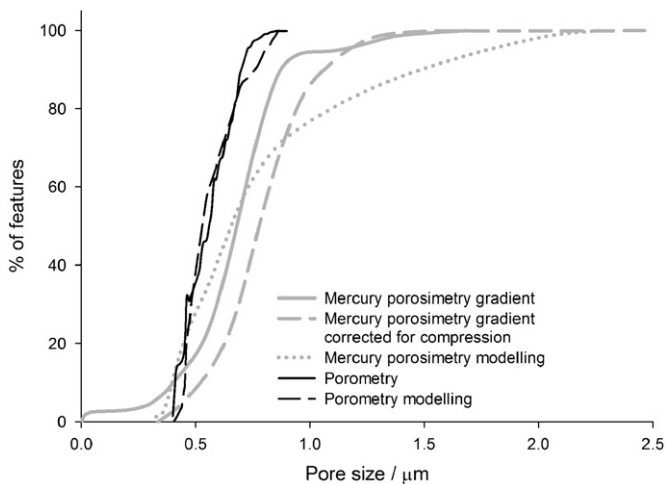


Fig. 8. Pore size distribution of a Whatman cellulose nitrate membrane filter determined by mercury porosimetry and porometry, together with the pore size distribution determined by modelling the porometry and mercury porosimetry data with Pore-Cor.

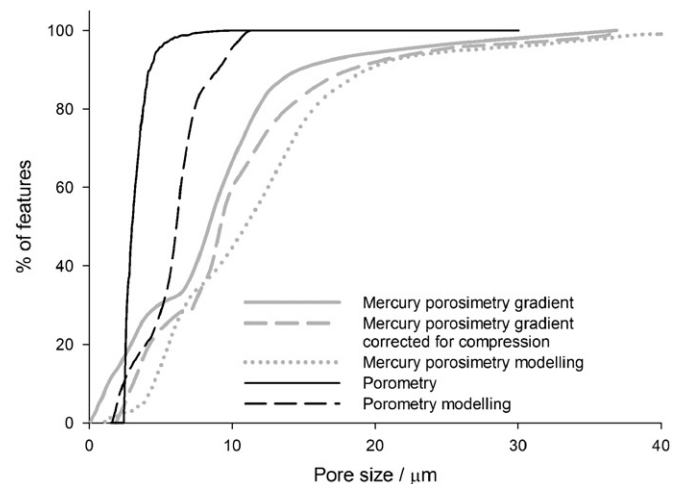


Fig. 9. Pore size distribution of grade 1 filter paper determined by mercury porosimetry and porometry, together with Pore-Cor modelling of mercury porosimetry and porometry.

Thus all porometers will give the correct measure of the sizes of track etch membranes, if used with their own proprietary fluids. Such agreement is often wrongly used to demonstrate the accuracy of the instruments. Nevertheless, once calibrated, porometry is shown to be a satisfactory method of measuring the filtration characteristics of filters with narrow size distributions, such as track etch membranes (Fig. 4), and cellulose membranes (Fig. 8). For filters with highly anisotropic structures with quaternary level structuring, such as the stainless steel filter (Figs. 7, S10 and S11) and glass fibre filter (Fig. 10 and S8) porometry reveals the filtration characteristics but gives no indication of holding capacity or the quaternary structure, i.e. the anisotropy of the holding characteristic to flow.

Mercury porosimetry is confirmed as a robust method of probing void structure, although interpretation by means of the gradient of the intrusion curve grossly underestimates the number of larger shielded voids within the structure. The sizes of these larger voids can be estimated using a void structure model which simultaneously fits the entire intrusion curve, matches the sample porosity and includes typical relationships between the

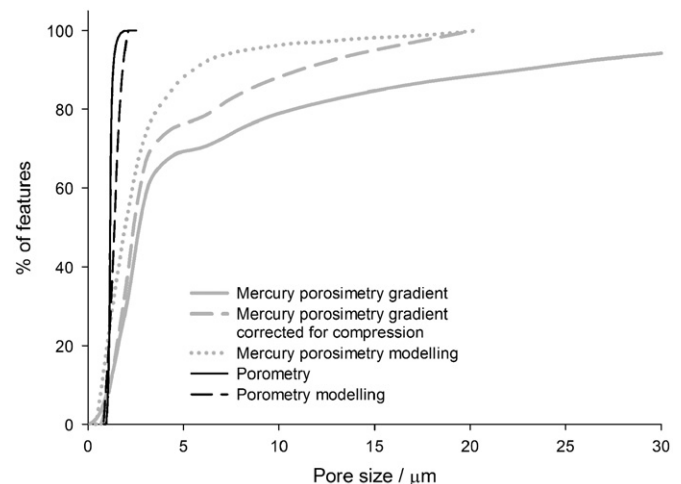


Fig. 10. Pore size distribution of a 0.7  $\mu\text{m}$  filtration-rated glass fibre filter determined experimentally using mercury porosimetry and porometry, and by modelling the experimental data.

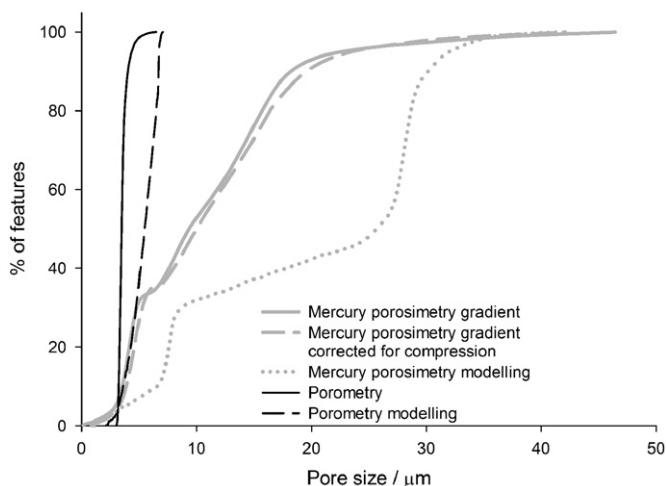


Fig. 11. Pore size distribution of stainless steel mesh filter 3AL3 determined by mercury porosimetry, porometry and pore size distribution modelled by Pore-Cor.

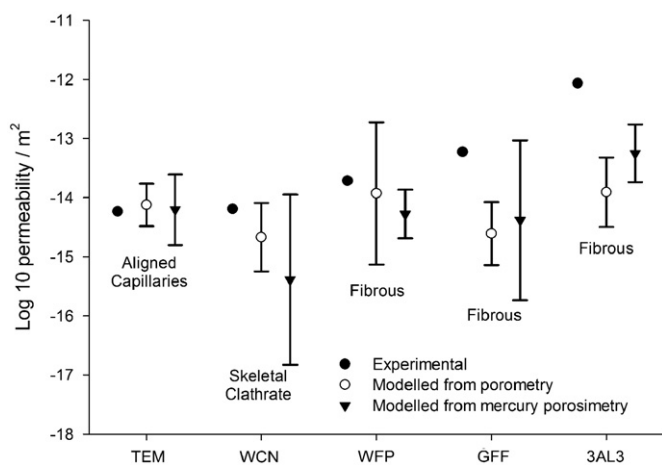


Fig. 12. Absolute gas permeabilities. Error bars represent two standard deviations. TEM: track etch membrane, WCN: Whatman cellulose nitrate membrane, WFP: Whatman grade 1 filter paper, GFF, glass fibre filter and 3AL3: stainless steel mesh filter.

sizes of pores and their adjoining throats. It has been shown that such a model can also be used to find the filtration characteristic from mercury porosimetry. The validity of the Cartesian model in this work is shown to break down for filters with complicated three-dimensional networks, such as woven and sintered fibre filters, in terms of the calculation of absolute permeability. Nevertheless for these more complicated structures it estimates the sizes of shielded voids, and also simulates the correct filtration characteristics.

## Acknowledgements

The authors wish to acknowledge Omya Development AG Switzerland, and the HEIF 3 program UK for funding the project. Omya Development AG is thanked for supporting cooperation between the University of Plymouth and its industrial Mineral and Surface Chemistry Research and Development. Porvair Filtration Group is thanked for the loan of a Porometer 4, and for collaboration in the development of its commercial control software.

## Appendix A. Supplementary materials

Supplementary data associated with this article can be found in the online version at doi:10.1016/j.ces.2011.05.013.

## References

- Calvo, J.I., Hernandez, A., Pradanos, P., Martinez, L., Bowen, W.R., 1995. Pore size distributions in microporous membranes. 2. Bulk characterization of track-etched filters by air porometry and mercury porosimetry. *Journal of Colloid and Interface Science* 176, 467–478.
- Dawe, R.A., Egbogah, E.O., 1978. Recovery of oil from petroleum reservoirs. *Contemporary Physics* 19, 355–376.
- Gane, P.A.C., Kettle, J.P., Matthews, G.P., Ridgway, C.J., 1996. Void space structure of compressible polymer spheres and consolidated calcium carbonate paper-coating formulations. *Industrial and Engineering Chemistry Research* 35, 1753–1764.
- Gane, P.A.C., Ridgway, C.J., Lehtinen, E., Valiullin, R., Furo, I., Schoelkopf, J., Paulapuro, H., Daicic, J., 2004. Comparison of NMR cryoporometry, mercury intrusion porosimetry, and DSC thermoporometry in characterizing pore size distributions of compressed finely ground calcium carbonate structures. *Industrial and Engineering Chemistry Research* 43, 7920–7927.
- Kumar, S., Chakarvarti, S.K., 2008. Measurement of average etched pore radius in ion track membranes through conductometric technique. *Modern Physics Letters B* 22, 2993–2998.
- Laudone, G.M., Matthews, G.P., Gane, P.A.C., 2008. Modelling diffusion from simulated porous structures. *Chemical Engineering Science* 63, 1987–1996.
- Laudone, G.M., Matthews, G.P., Gane, P.A.C., Ridgway, C.J., Schoelkopf, J., 2005. Estimation of the effective particle sizes within a paper coating layer using a void network model. *Chemical Engineering Science* 60, 6795–6802.
- Li, D.P., Frey, M.W., Joo, Y.L., 2006. Characterization of nanofibrous membranes with capillary flow porometry. *Journal of Membrane Science* 286, 104–114.
- Lowell, S., Shields, J.E., Thomas, M.A., Thommes, M., 2004. *Characterization of Porous Solids and Powders: Surface Area, Pore Size and Density*. Kluwer Academic Publishers, Netherlands.
- Matthews, G.P., Canonville, C., Moss, A.K., 2006. Use of a void network model to correlate porosity, mercury porosimetry, thin section, absolute permeability and NMR relaxation time data for sandstone rocks. *Physical Review E* 73 (art 031307).
- Matthews, G.P., Laudone, G.M., Gregory, A.S., Bird, N.R.A., Matthews, A.G., Whalley, W.R., 2010. Measurement and simulation of the effect of compaction on the pore structure and saturated hydraulic conductivity of grassland and arable soil. *Water Resources Research* 46, W05501.
- Matthews, G.P., Moss, A.K., Ridgway, C.J., 1995. The effects of correlated networks on mercury intrusion simulations and permeabilities of sandstone and other porous media. *Powder Technology* 83, 61–77.
- Meyers, J.J., Crosser, O.K., Liapis, A.I., 2001. Pore network modelling: determination of the dynamic profiles of the pore diffusivity and its effect on column performance as the loading of the solute in the adsorbed phase varies with time. *Journal of Chromatography A* 908, 35–47.
- MiettonPeuchot, M., Condat, C., Courtois, T., 1997. Use of gas–liquid porometry measurements for selection of microfiltration membranes. *Journal of Membrane Science* 133, 73–82.
- Mourhatch, R., Tsotsis, T.T., Sahimi, M., 2011. Determination of the true pore size distribution by flow permporometry experiments: an invasion percolation model. *Journal of Membrane Science* 367, 55–62.
- Peat, D.M.W., Matthews, G.P., Worsfold, P.J., Jarvis, S.C., 2000. Simulation of water retention and hydraulic conductivity in soil using a three-dimensional network. *European Journal of Soil Science* 51, 65–79.
- Price, J.C., Matthews, G.P., Quinlan, K., Sexton, J., Matthews, A.G.D., 2009. A depth filtration model of straining within the void networks of stainless steel filters. *AIChE Journal* 55, 3134–3144.
- Rasband, W.S., 2008. *ImageJ*, 1.42o ed. U.S. National Institutes of Health, Bethesda, Maryland, USA.
- Ravikovitch, P.I., Neimark, A.V., 2002. Experimental confirmation of different mechanisms of evaporation from ink-bottle type pores: equilibrium, pore blocking, and cavitation. *Langmuir* 18, 9830–9837.
- Ridgway, C.J., Gane, P.A.C., 2002. Dynamic absorption into simulated porous structures. *Colloids And Surfaces A-Physicochemical And Engineering Aspects* 206, 217–239.
- Ridgway, C.J., Schoelkopf, J., Matthews, G.P., Gane, P.A.C., James, P.W., 2001. The effects of void geometry and contact angle on the absorption of liquids into porous calcium carbonate structures. *Journal of Colloid and Interface Science* 239, 417–431.
- Rigby, S.P., 2000. A hierarchical structural model for the interpretation of mercury porosimetry and nitrogen sorption. *Journal of Colloid and Interface Science* 224, 382–396.
- Rigby, S.P., Chigada, P.I., 2010. MF-DFT and experimental investigations of the origins of hysteresis in mercury porosimetry of silica materials. *Langmuir* 26, 241–248.
- Rigby, S.P., Daut, S., 2002. A statistical model for the heterogeneous structure of porous catalyst pellets. *Advances in Colloid and Interface Science* 98, 87–119.

- Rigby, S.P., Fletcher, R.S., Raistrick, J.H., Riley, S.N., 2002. Characterisation of porous solids using a synergistic combination of nitrogen sorption, mercury porosimetry, electron microscopy and micro-focus X-ray imaging techniques. *Physical Chemistry Chemical Physics* 4, 3467–3481.
- Sel, O., Sallard, S., Brezesinski, T., Rathouski, J., Dunphy, D.R., Collord, A., Smarsly, B.M., 2007. Periodically ordered meso- and macroporous SiO<sub>2</sub> thin films and their induced electrochemical activity as a function of pore hierarchy. *Advanced Functional Materials* 17, 3241–3250.
- Solcova, O., Matejova, L., Schneider, P., 2006. Pore-size distributions from nitrogen adsorption revisited: models comparison with controlled-pore glasses. *Applied Catalysis A-General* 313, 167–176.
- Thommes, M., Skudas, R., Unger, K.K., Lubda, D., 2008. Textural characterization of native and n-alkyl-bonded silica monoliths by mercury intrusion/extrusion, inverse size exclusion chromatography and nitrogen adsorption. *Journal of Chromatography A* 1191, 57–66.
- Tsakiroglou, C.D., Ioannidis, M.A., Amirtharaj, E., Vizika, O., 2009. A new approach for the characterization of the pore structure of dual porosity rocks. *Chemical Engineering Science* 64, 847–859.
- van Brakel, J., Modry, S., Svata, M., 1981. Mercury porosimetry: state of the art. *Powder Technology* 29, 1–12.
- Wallqvist, V., Claesson, P.M., Swerin, A., Ostlund, C., Schoelkopf, J., Gane, P.A.C., 2009. Influence of surface topography on adhesive and long-range capillary forces between hydrophobic surfaces in water. *Langmuir* 25, 9197–9207.
- Ziel, R., Haus, A., Tulke, A., 2008. Quantification of the pore size distribution (porosity profiles) in microfiltration membranes by SEM, TEM and computer image analysis. *Journal of Membrane Science* 323, 241–246.